

# Peristaltic piezoelectric micropump system for biomedical applications

Ling-Sheng Jang · Wai-Hong Kan

Published online: 16 May 2007  
© Springer Science + Business Media, LLC 2007

**Abstract** This study presents a peristaltic piezoelectric micropump system to transport deionized water and whole blood, and deliver phosphated buffered saline (PBS) into the vein of a rat, thus simulating insulin injections for diabetes. The proposed system comprises a micropump, a 12 V battery, an ATmega 8535 microprocessor, a 12–180 V DC-to-DC converter based on transformerless technology, three differential amplifiers, an IC 7805, a phase controller, an A/D converter, a keyboard and an LCD module. The system can generate step-function signals of the 3-, 4-, and 6-phase actuation sequences with voltages of up to  $228 V_{pp}$  ( $\pm 114$  V) and frequencies ranging from 10 Hz to 100 kHz, as the inputs for the pump. It is portable and programmable with a package size of  $22 \times 12.8 \times 9$  cm. Additionally, a protocol of the PEOU (N-(triethosilylpropyl)-O-polyethylene oxide urethane) coating is developed to form a self-assembly monolayer, thus increasing the hemocompatibility of the micropump, and keeping blood flowing smoothly through the micropump without blocking. This study performs the circuit testing and fluid pumping, and reveals the effects of actuation sequences and liquid on pump performance. The flow rates for pumping DI water and whole blood are 16.6–121.6  $\mu\text{l}/\text{min}$  and 8.6–50.2  $\mu\text{l}/\text{min}$ , respectively when the voltages are changed from  $80 V_{pp}$  ( $\pm 40$  V) to  $140 V_{pp}$  ( $\pm 70$  V). And the maximum backpressures are 3.2 and 1.8 kPa for DI water and whole blood at  $150 V_{pp}$  ( $\pm 75$  V), respectively. The mean artery pressure (MAP) and heart rates of the rate are 63–69 mmHg and

266–279 beats/min, respectively, throughout the injection process, indicating an insignificant change in physiological reactions of rats.

**Keywords** Peristaltic micropump · Piezoelectric · Driving system · Blood transportation · Physiological observation

## 1 Introduction

Micropumps, microvalves, micromixers and micro-flow sensors have been extensively developed to manipulate fluids in the micro scale (Cao et al. 2001; Liao et al. 2005). The micropump is a major component of such devices owing to its significant potential in biological applications (Laser and Santiago 2004). Various micropumps have been investigated in the last decade. Various actuation principles, such as piezoelectrics (Andersson et al. 2001), shape memory alloys (Shu 2002), electrostatics (Xie et al. 2004; Francois and Dufour 1998), thermal actuation (Tsai and Lin 2002) and magnetics (Ahn and Allen 1995), have been adopted to develop micropumps. Nonetheless, piezoelectric actuation is promising due to its simple structure, high output power density and high actuation strength (Nguyen et al. 2002).

Most reported micropumps are reciprocating displacement pumps with a diaphragm as the moving surface. These are known as membrane pumps or diaphragm pumps. Peristaltic pumps are reciprocating displacement micropumps in which the active valves and the primary chamber have the same form factor (Smits 1990). The peristaltic-type actuators can be used as active valves, and controlled easily with the applied input power with no additional fabrication process for the valves. The pumping principle is

L.-S. Jang (✉) · W.-H. Kan  
Department of Electrical Engineering and Center for Micro/Nano Science and Technology, National Cheng Kung University,  
1 University Road, Tainan 701, Taiwan  
e-mail: lsjang@ee.ncku.edu.tw

based on the peristaltic motion of the diaphragms, which squeezes the fluid in the required direction. The peristaltic pumps theoretically need three or more reciprocating membranes. The pumping of both air and water in microfluidic channels has been successfully demonstrated in peristaltic pumps (Husband et al. 2004; Lee et al. 2004; Jan 1990). These peristaltic pumps are bubble-tolerant, and are capable of self-priming and bidirectional transportation.

Portable micro devices are currently gaining attention, since they have many potential applications in fields requiring portability. However, the driving equipment of peristaltic pumps based on piezoelectric actuators is usually bulky, cumbersome, hard to carry and difficult to combine with other components. Hence, a stand-alone driving circuit for the peristaltic micropump is needed to achieve portability and integration.

Analyzing the properties of patient blood is crucial to accurate diagnosis. The demand is increasing since it is believed to improve the quality of life. Recent MEMS technology can be adopted to reduce the total size of the blood test system, at a reasonable overall cost. However, whole blood coagulates within a few seconds of contact with a silicon surface. Hence, most experiments adopt control blood on micro-devices. For instance, polystyrene latex particles and a diluted solution of the control blood have been used in MEMS devices (Satakea et al. 2002; Tanabe et al. 2006; Takaoa et al. 2005).

This study presents a peristaltic micropump system based on piezoelectric actuation to transport deionized water and whole blood, and to deliver phosphated buffered saline (PBS) into the vein of a rat, thus simulating insulin injections for diabetes. A driving system based on a micro-processor, and supplied by a 12 V battery, was developed to drive three piezoelectric actuators. Three actuation sequences were designed to examine pump performance. Additionally, the micropump driving system was improved by adding a negative bias field to the driving voltage, thus increasing the displacement of the diaphragm and the flow rates. Moreover, the micropump was coated with a SAM (self-assembly monolayer) to prevent blood from coagulating.

## 2 Design and fabrication

The peristaltic micropump consists of silicon, Pyrex glass and three commercially available bulk PZT chips (Bu et al. 2003). The Pyrex glass was etched to form a 200  $\mu\text{m}$  thick pump diaphragm by a photolithography process with 49% HF. The inlet and outlet were drilled through the patterned Pyrex glass with a diamond bit. The pump channels and chambers were fabricated on the silicon substrate using the two-level etched process. First, a layer of 3,000  $\text{\AA}$

aluminum was sputtered onto the silicon, which was (100) oriented with a thickness of 500  $\mu\text{m}$ . Second, the channels were patterned using a photolithography process, Al etchant and deep reactive ion etching (DRIE), which etched the silicon with a depth of 170  $\mu\text{m}$ . Third, the chambers were patterned with a depth of 30  $\mu\text{m}$  by the channel fabrication process. Hence, the channels and chambers were etched at depths of 200 and 30  $\mu\text{m}$ , respectively. The diameters of the three chambers were 12 mm. The Pyrex membrane was bonded to the patterned silicon substrate with anodic bonding at 475°C and 1,000 V. Three 12×12 mm PZT chips (PIEZO SYSTEMS, INC., T107-H4E-602) with a thickness of 191  $\mu\text{m}$  were then attached to the glass diaphragm using silver epoxy (EPO-TEK, H31). Figure 1 schematically illustrates the peristaltic pump. The inlet and outlet tubes, and an electric connector were fixed on the device by epoxy. The package size of the pump, which included Pyrex, silicon and bulk PZT chips, was 75×24×1.1 mm.

To prevent blood from clotting on the micro-device, a SAM, N-(triethosilylpropyl)-O-polyethylene oxide urethane (PEOU, MW = 400–500, Gelest, Inc.) was adopted to form a monolayer on the chip surface. The monolayer consists of long carbon chains, which are hydrophobic, and can prevent direct contact between whole blood and pump surfaces. First, the surfaces of pump channels and chambers were cleaned by DI water, ethanol and an oxidant solution with HCl:H<sub>2</sub>O<sub>2</sub>:DI water (1:1:6 V), in that order. The pump was then placed in an oven at 75°C. Second, the PEOU was dissolved into a tetrahydrofuran (THF) solution (Miqin et al. 1998; Oha et al. 2004). The PEOU solution was introduced into the pump at room temperature for 24 h. The pump was then immersed into PEOU solution, and sealed with tin foil to prevent the toluene from evaporating. Finally, the pump was rinsed with THF, and dried in a stream of nitrogen.

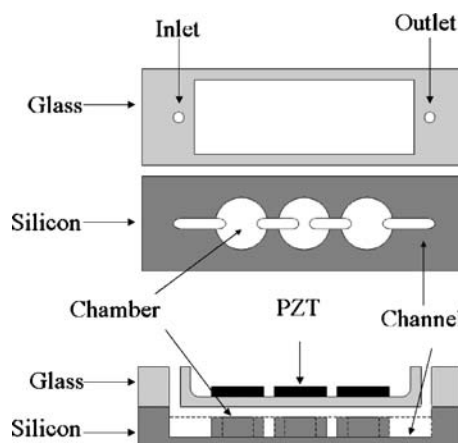


**Fig. 1** Schematic of the peristaltic micropump

### 3 Principles of actuation sequences

The piezoelectric peristaltic micropump with three chambers connected in series is operated in a peristaltic motion. The driving circuits actuate the PZT chips to deflect the diaphragm with an oscillating motion. The peristaltic motion induces the pumping of fluid in the chambers when three diaphragms are actuated by an actuation sequence. The control signals of three diaphragms are generated to attain peristaltic motion with three differential amplifiers and a phase controller. This study designed and used three different actuation sequences to investigate pump performance. Figure 2 shows the 6-phase actuation sequence, 100-110-010-001-000. The logical “1” is defined as the up motion of the PZT disk, which pulls the Pyrex diaphragm up to draw the fluid into the chamber, and the logical “0” is defined as the down motion of the PZT disk, which pushes the Pyrex diaphragm down, thus displacing the fluid from the chamber. In the 6-phase sequence, the fluid is drawn into the pump in steps 1–3, and then pumped out in step 4–6. The 4-phase sequence skips two steps of the 6-phase sequence, and is 100-110-011-001. The 3-phase sequence, which skips three steps of the 6-phase sequence, is 100-010-001.

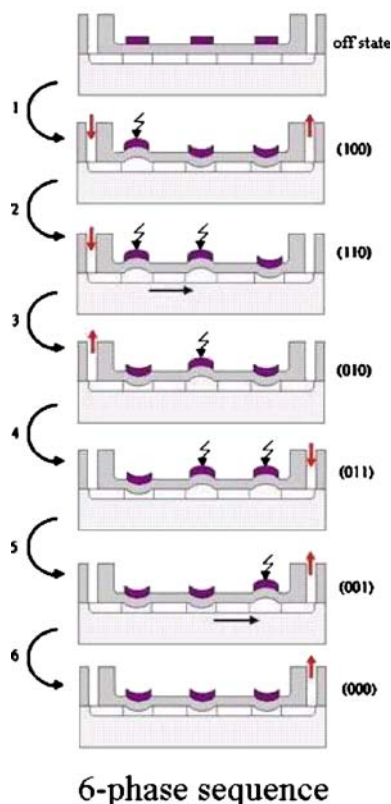


**Fig. 2** The 6-phase actuation sequence of a peristaltic micropump with PZT actuators

The pump can be considered as a simple spring–mass–damper system under harmonic excitation. This can be treated as a Helmholtz resonator or as a mass–spring system,

$$M\ddot{y} + ky = \bar{F} \sin(\omega t) - F_{\text{chamber}} \quad (1)$$

where  $M$  and  $k$  denote mass and spring constant, respectively. The bi-layer “piezoelectric disk and Pyrex glass diaphragm” are defined as the diaphragm. In this case, the spring is the diaphragm. The frequency at which the amplitude–response curve is a maximum called the damped natural frequency,  $\omega_d$  can be expressed as Eq. 2,

$$\omega_d = \omega_n \sqrt{1 - 2\zeta^2} = \omega_n \sqrt{1 - \frac{c^2}{Mk}} \quad (2)$$

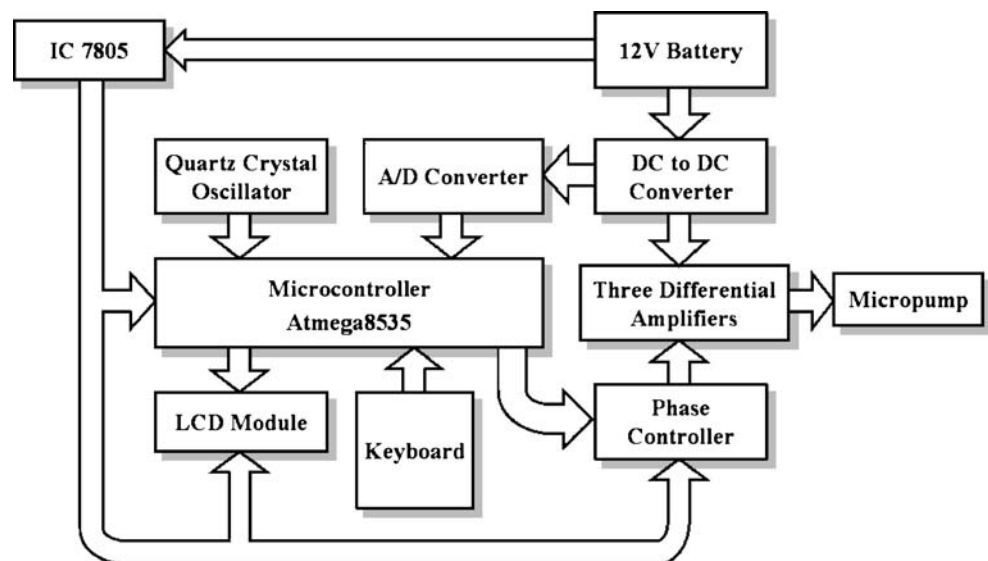
where  $\omega_n = \sqrt{\frac{k}{M}}$  represents the natural frequency of the diaphragm in a vacuum, and  $\zeta = \frac{c}{2\sqrt{Mk}}$  denotes the damping factor (Timoshenko and Weaver 1974), which is considered to change the natural frequency of the actuating diaphragm in a vacuum. The parameter  $c$  denotes the added damping constant.

### 4 Design of the driving circuits

The driving system comprises an ATmega 8535 microprocessor, a 12 V battery, a 12–180 V DC-to-DC converter, an IC 7805, three differential amplifiers, a phase controller, a keyboard, an A/D converter and an LCD screen. Figure 3 depicts the block diagram of the system. The microprocessor with high-performance and low-power AVR<sup>®</sup> 8-bit microcontroller manufactured by ATMEL is the major component of the system. The microprocessor has several functions, such as a self-programming memory, multiple instructions and a debugging interface. The code is written in the C language, and embedded in the microprocessor. The LCD module receives character codes from the microprocessor, and stores them in its display data RAM. Each character code is then converted into a character, which is displayed on the screen. The A/D conversion is performed with a CMOS 8-bit successive approximation A/D converter (ADC0804). The A/D converter transforms an analog DC voltage from the output of a 12–180 V DC-to-DC converter into a digital value with successive approximation. The values of the voltage from the A/D converter and frequency from the microprocessor are then displayed on the LCD module.

The 12–180 V DC-to-DC converter is based on transformerless technology, and produces a high output voltage (Rodes 2004). The DC-to-DC converter consists of 18 voltage-doubler cells cascaded in a chain-like structure to produce 180 V from a 12 V battery. Each cell includes

**Fig. 3** Block diagram of the stand-alone driving system



a diode, a capacitor and a Schmitt-trigger inverter (CD40106B). The push–pull stage of the Schmitt-trigger inverter is obtained from two complementary MOSFETs. The clock signal is generated with a 1 k $\Omega$  resistor in series with a 100 pF capacitor in the first cell, and produces a 0–12 V square wave at 150 kHz. At the end of one push–pull stage, the output of the first cell becomes  $V_{\text{out-cell}} = 2V_{\text{DD}} - 2V_{\text{D}}$ , where  $V_{\text{DD}}$  denotes the supply voltage, and  $V_{\text{D}}$  represents the forward-voltage drop of  $D_1$  (about 0.7 V). Thus, the DC-to-DC converter yields  $V_{\text{OUT}} = (N+1)(V_{\text{DD}} - V_{\text{D}})$  when  $N$  voltage-doubler cells are cascaded in the chain-like structure. The number of voltage-doubler cells, given by  $N$  to maximize the high output voltage, is determined based on the above principle. The generated high-output voltage is provided to the differential amplifiers.

The differential amplifier is operated as a switching circuit (Carr and Brown 2001). The amplitude of the output signal is twice that of the input signals when two transistors are excited by two reverse signals. The circuit does not require two bias sources to generate a high voltage. Additionally, the circuit with a single bias source consumes less power than that with two bias sources. The differential amplifier has several advantages, including high voltage output, single bias source and elimination of noise, and is appropriate for driving the pump, requiring a high voltage. The circuits of the three differential amplifiers are designed to excite three PZT chips in the 3-, 4- or 6-phase peristaltic motion by managing six signals produced by the phase controller.

The phase controller, which consists of three clocked D flip-flops controlled by the microprocessor, generates the signals to the input terminals of the differential amplifiers. The output of the D flip-flop follows the input of the D flip-flop when the positive edge-triggered event occurs. Three D flip-flops are integrated with AND gates and OR gates to construct the logical circuits of the 3-, 4-, and 6-phase

actuation sequences. The number of boolean expressions is minimized by a Karnaugh map. The phase controller is successfully developed using the boolean equations to generate the 3-, 4- and 6-phase actuation sequences. The completed circuit box is 22 $\times$ 12.8 $\times$ 9 cm. This system can produce step-function signals with a voltage of up to 228  $V_{\text{pp}}$  ( $\pm 114$  V), and a frequency from 10 Hz to 100 kHz as the inputs of the pump.

## 5 Experimental results and discussion

### 5.1 Circuit testing

The driving system was tested with a loaded and unloaded pump. According to the experiments, the circuits accurately generated the 3-, 4- and 6-phase actuation sequences, which were 100-010-001, 100-110-011-001 and 100-110-010-011-001-000, respectively. The high voltage power supply and differential amplifiers of the driving system produced a stable voltage of 228  $V_{\text{pp}}$  ( $\pm 114$  V). The maximum output voltage was decreased from 228  $V_{\text{pp}}$  ( $\pm 114$  V) to 212  $V_{\text{pp}}$  ( $\pm 106$  V) at 100 Hz when the pump was loaded. This loading effect was associated with the maximum power output of the DC-to-DC converter. Additionally, the rise and falling times in the waveform of the driving signal were both 2.742 ms, due to the charging and discharging periods of the capacitive elements. The capacitive effect of the pump was caused by the capacitive characteristic of the PZT chips.

The power consumption was measured when the pump was actuated by the 3-, 4- and 6-phase sequences. The power consumption of the driving circuits was measured from the current  $I_{\text{in}}$  drawn from the 12 V battery. The total power delivered to the load is expressed as  $P_{\text{T}} = 12 V \cdot I_{\text{in}}$ .

The load comprised three differential amplifiers, an IC 7805, a phase controller, a keyboard, an A/D converter, an ATmega microprocessor, LCD and the peristaltic micro-pump. The power consumption of the system was around 683 mW when the pump was operated at 100 Hz and 140 V<sub>pp</sub> (±70 V).

### 5.2 Pump performance

To evaluate the pump performance, the pump was excited in 3-, 4- and 6-phase peristaltic motions, and actuated with the step-function signals with varied driving voltages and frequencies generated by the driving system. Two 0.04-in. ID tubes were linked to the inlet and outlet of the peristaltic micropump. The outlet tube was placed into a reservoir on a scale. The pumping rates were computed over a period of time from the weight of deionized water (DI water), measured with the scale. The maximum displacement of

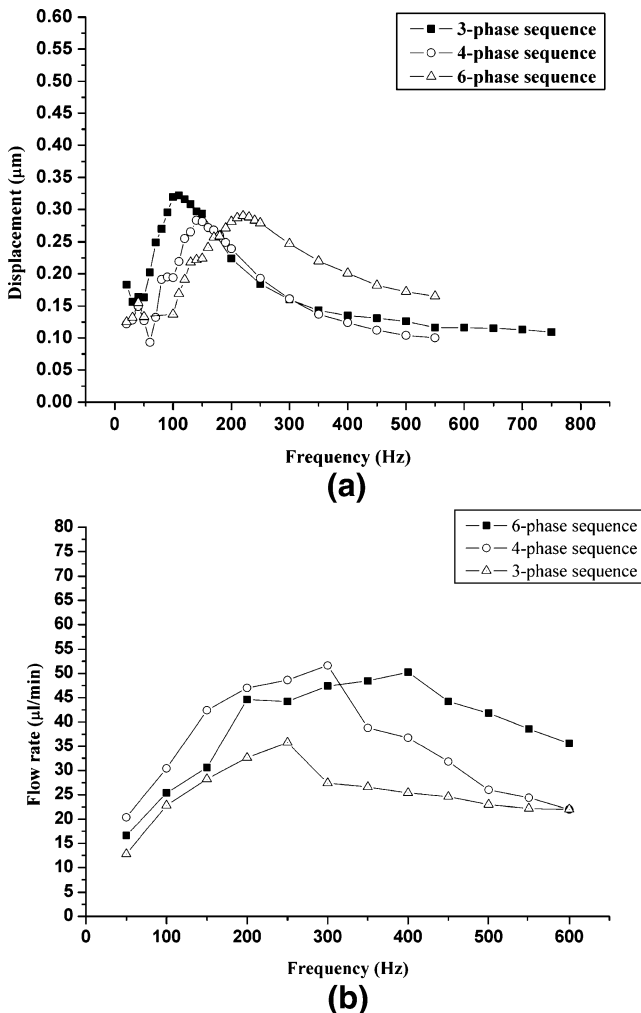


**Fig. 4** (a) Displacement of the middle diaphragm against frequency (b) flow rate against frequency at 100 V<sub>pp</sub> (±50 V) in 3-, 4- and 6-phase sequences

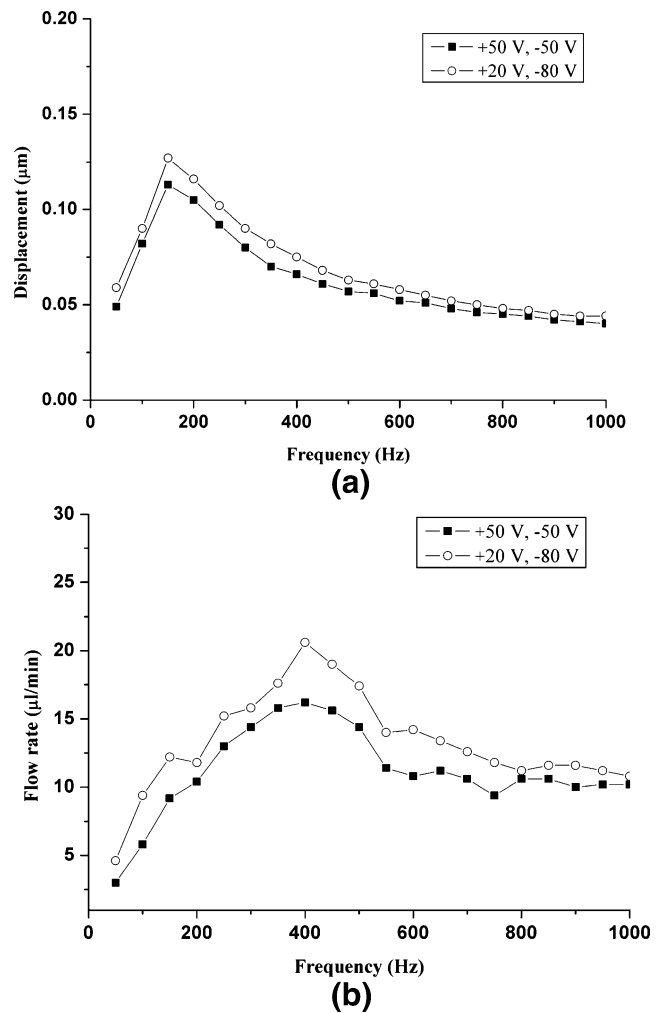


**Fig. 5** (a) Displacement vs. frequency (b) flow rate vs. frequency at 100 V<sub>pp</sub> from +50 to -50 V and +20 to -80 V in the 4-phase sequence

the diaphragm with DI water was measured using a fiber-optical measurement system (MTI Instruments, MTI 2000), which has an accuracy within 1.0% for peak-to-peak readings from 1 Hz to 150 kHz, and which acted as a displacement sensor to monitor the dynamic performance of the pump. The signals from the fiber-optical measurement system were stored by a digital oscilloscope. Pump performance at nonzero back pressure was determined when the outlet reservoir on the scale was elevated to a certain height using a vertical linear stage (DOCLJ-1, SIGMA KOKI CO., LTD.). The experimental results reveal that bidirectional flow can be achieved by reversing the actuation sequence.

Figure 4(a) shows the displacement of the middle diaphragm as a function of phase frequency at 100 V<sub>pp</sub> (±50 V) for the 3-, 4- and 6-phase sequences. The figure indicates that different actuation sequences result in different operating frequencies of the diaphragm. The resonant frequencies of the diaphragm for the 3-, 4- and

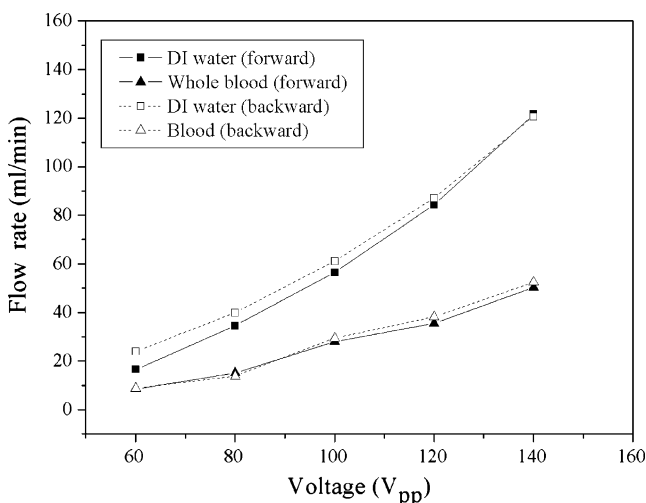
6-phase sequences were 110, 140 and 220 Hz, respectively. The maximum displacement of the diaphragm for the 3-, 4- and 6-phase actuation sequences were 0.32, 0.28 and 0.29  $\mu\text{m}$  (peak-to-peak), respectively.

Figure 4(b) shows the flow rates of the micropump at an applied voltage of 100  $V_{pp}$  ( $\pm 50$  V) with a phase frequency range of 50–600 Hz for the 3-, 4- and 6-phase peristaltic motions. The maximum flow rates of the 3-, 4- and 6-phase sequences occurred at 250, 300 and 400 Hz, and were 35.8, 51.6 and 50.2  $\mu\text{l}/\text{min}$ , respectively. According to Fig. 4(b), the flow rates for all actuation sequences peaked at a particular frequency and fell at higher frequencies.

Figure 5(a) and (b) plot the displacement of the diaphragm and flow rate vs. frequency at 100  $V_{pp}$  for two outputs from +50 to  $-50$  V, and from +20 to  $-80$  V in the 4-phase actuation sequence. Experimental results show that the maximum displacement and flow rate improved from 0.11 to 0.13  $\mu\text{m}$  (peak-to-peak) and 16.2 to 20.6  $\mu\text{l}/\text{min}$ , respectively, when a negative dc bias was applied to the PZT actuators. According to Masys et al. (2003), the piezoelectric constant relating to the mechanical strain generated by an applied electric field rises when an additional negative bias field (along the poling direction) is applied to the well-poled hard PZT. A negative dc bias results in field-induced deaging, which is a depinning of the domain walls, and which increases the extrinsic contribution to the piezoelectric response. Therefore, the displacement of the diaphragm rises with the piezoelectric constant, thus increasing the flow rates.

### 5.3 Pumping whole blood

A blood transportation test was first performed to evaluate the adequacy of the PEOU coating. The blood samples



**Fig. 6** Forward and backward flow rates of the micropump for DI water and whole blood in the 4-phase sequence at 500 and 450 Hz, respectively

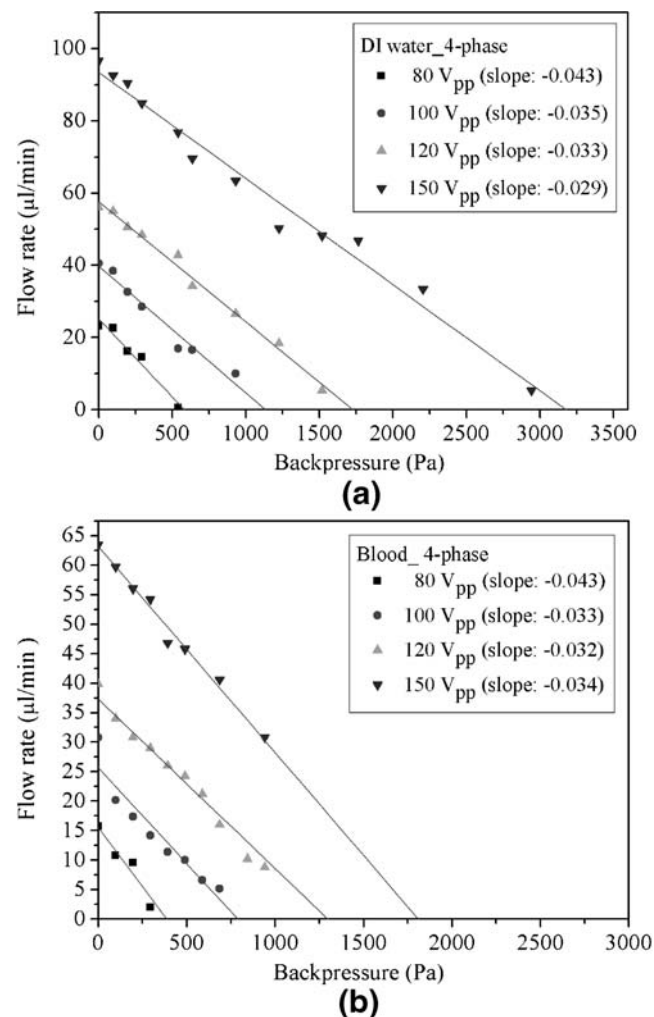


**Fig. 7** Flow rates vs. backpressure of (a) DI water (b) whole blood in the four-phase sequence

were supplied by the blood bank of Chi Mei Hospital in Taiwan. They were collected in containers with heparin (AGGLUTEX, HEPARIN 5000 u/l ml). A syringe pump was used to drive the whole blood into the micropump coated with PEOU at a constant flow speed of 4.2 ml/h. The experiment demonstrates that the blood flowed through the PEOU-coated micropump without clotting for more than 30 min. For comparison, the same configuration with an untreated micropump was also adopted. However, this pump jammed within a few seconds. Based on this experiment, PEOU was the preferred interface between silicon surface and blood, thus increasing the hemocompatibility of the micropump and keeping blood flowing smoothly through the micropump without blocking.

Figure 6 plots the forward and backward pumping rates in the 4-phase sequence for DI water and whole blood at operating frequencies of 500 and 450 Hz, respectively. In the pumping mode, the peristaltic micropump could transport liquids either forward or backward by reversing

the actuation sequence. The diaphragm with whole blood as the working medium had a damped natural frequency lower than that with deionized water as the working medium, since blood is more viscous than water. Additionally, the flow rates of the whole blood were lower than those of water due to the fluid viscosity. Figure 6 indicates that both forward and backward flow rates approached a linear curve, and that the flow rate rose steadily with the voltage. The flow rates of DI water and whole blood were 16.6–121.6  $\mu\text{l}/\text{min}$  and 8.6–50.2  $\mu\text{l}/\text{min}$ , respectively when the voltages were changed from 80  $V_{\text{pp}}$  ( $\pm 40$  V) to 140  $V_{\text{pp}}$  ( $\pm 70$  V). The backpressure is an index of a pump's performance. Four different voltages were applied in DI water and whole blood transportation. The flow rates were measured with increasing backpressure. Figure 7 shows that the maximum backpressures were 3.2 and 1.8 kPa for DI water and whole blood, respectively. That is, the maximum heights that the micropump could reach were 32.6 and 18.3 cm for DI water and whole blood, respectively. The results demonstrate that the liquid strongly influences pump performance.

#### 5.4 Physiological observation of PBS injection into a rat

The physiological effects of all clinical instruments on the body have to be studied carefully. The instruments could also affect the medical treatment, in particular large-scale instruments, and rarely-used silicon-based devices such as micropumps. Hence, the PBS injection by the developed micropump was conducted to discover the physiological responses of the animal under testing.

Rats that weighed 500 g were used to evaluate the behavior of the micropump in transporting PBS. The rat under test was anesthetized with 1 ml Urethan and the light bulb kept the rat warm to prevent hypothermia during testing. The inlet and outlet of micropump were connected to the femoral artery and vein of rats, respectively. The physiological functions of the animals were recorded using a blood pressure and heart rate monitor (ADInstruments, PowerLab/8P). The duration of infusion at each voltage was five minutes.

This test measured two physiological parameters of the rat, namely mean artery pressure (MAP) and heart rate. All data were estimated as averages over 5 min. Blood pressure varies continuously, and comprises systolic and diastolic pressure. Either systolic or diastolic pressures alone can be applied to diagnose cardiovascular diseases, but cannot elucidate physiological responses to environmental effects. Hence, MAP, rather than single systolic or diastolic pressure, was chosen to estimate the effect of PBS injection resulting from the micropump. MAP equals one-third of systolic pressure plus two thirds of diastolic pressure, and is often adopted to evaluate the response of the body in medical research. Figure 8 plots MAP at various applied

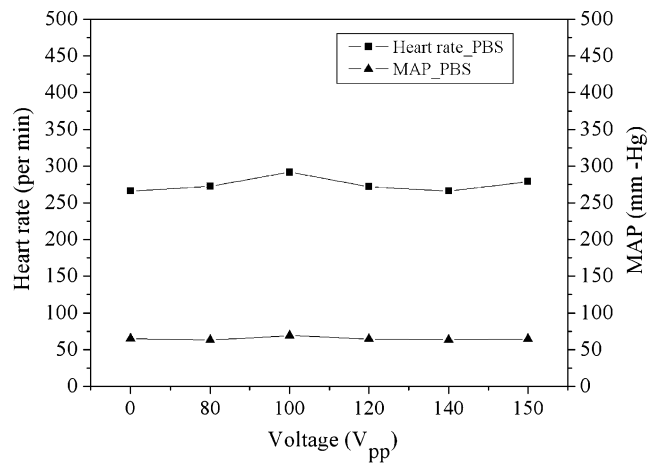


**Fig. 8** Heart rates and MAP of the rat at various applied voltages in the four-phase actuation sequence

voltages in the range 0–150  $V_{\text{pp}}$  ( $0\text{--}\pm 75$  V). During the PBS injection process, MAP was initially 65 mmHg when no electrical signal was applied to the pump. The MAP was 63–69 mmHg throughout the process, indicating an insignificant change in the blood pressure of the rat. Figure 8 also summarizes the heart rates of the rat when various voltages were applied. The heart of a small animal beats more quickly than that of a human being—generally between 200 and 300 beats/min. During the PBS injection process, the heart rate rose when the electric signal was initially applied, reaching a maximum value of 279 when 100  $V_{\text{pp}}$  ( $\pm 50$  V) was applied to the pump. The total variance was below 13 beats/min (between 266 and 279), and did not significantly influence the physiological functioning of the rat. The application of the micropump was found not to induce a severe physiological reaction in the rat, based on the blood pressure and heart beat at current conditions.

## 6 Conclusions

A stand-alone micropump system, comprising a peristaltic micropump, a 12 V battery, an ATmega 8535 microprocessor, a 12 V–180 V DC-to-DC converter, an IC 7805, three differential amplifiers, a phase controller, an A/D converter, a keyboard and an LCD module, was successfully developed. This battery-based driving system, combined with the 3-, 4- and 6-phase actuation sequences, demonstrated bidirectional fluid pumping with DI water and whole blood. The loading effect of the micropump reduced the maximum output voltage of the circuits from 228  $V_{\text{pp}}$  ( $\pm 114$  V) to 212  $V_{\text{pp}}$  ( $\pm 106$  V) at 100 Hz. The rising and falling times in the waveform of the driving signal were both 2.742 ms. The power consumption of the system was about 683 mW when the pump was operated at 100 Hz and

140 V<sub>pp</sub> ( $\pm 70$  V). Additionally, the experimental results indicate that different actuation sequences led to different resonant frequencies of the diaphragm. The resonant frequencies of the diaphragm for the 3-, 4- and 6-phase sequences were 110, 140 and 220 Hz at a driving voltage of 100 V<sub>pp</sub> ( $\pm 50$  V), respectively. This study also indicates that adding a negative dc bias to the driving voltage enhanced the displacement of the diaphragm and the flow rates. Moreover, a protocol of the PEOU coating was successfully developed to increase the hemocompatibility of the micropump, and keep blood flowing through the micropump smoothly without blocking. The flow rates of DI water and whole blood at 140 V<sub>pp</sub> ( $\pm 70$  V) in the 4-phase sequence were 121.6 and 50.2  $\mu\text{l}/\text{min}$ , respectively. The maximum backpressures at 140 V<sub>pp</sub> ( $\pm 70$  V) in the 4-phase sequence were 3.2 and 1.8 kPa for DI water and whole blood, respectively. The flow rates and backpressure of whole blood were less than those of DI water due to the fluid viscosity. The results show that the liquid strongly affects pump performance. Furthermore, a physiological observation of the PBS injection into the vein of a rat was performed to simulate the insulin injection for diabetes. The MAP and heart rates of the rat throughout the injection process were 63–69 mmHg and 266–279 beats/min, respectively, representing an insignificant change in physiological reactions of the rat. In future work, an equivalent electrical model of the PZT actuator will be developed to optimize the dimensions of actuators and improve the driving circuits. Additionally, a mathematical model of the peristaltic micropump based on piezoelectric actuation including actuation sequences, operating frequency, diaphragm diameter and chamber depth will be constructed to enhance the pump performance.

**Acknowledgements** This work was supported by the National Science Council (NSC 94-2215-E-006-051) and Chi Mei Hospital of Taiwan (CMFHR9421). Additionally, this work made use of Shared Facilities supported by the Program of Top 100 Universities Advancement, Ministry of Education, Taiwan. The authors also would like to thank the Center for Micro/Nano Science and Technology, National Cheng Kung University, and National Nano Device

Laboratories, Tainan, Taiwan, for equipment access and technical support. Moreover, the authors would like to thank Dr. Ching-Cheng Hou's assistance for animal tests in Chi Mei Hospital.

## References

- C.H. Ahn, M.G. Allen, in *Proceedings of the IEEE Micro Electro Mechanical Systems (MEMS)*, 1995, pp. 408–412
- H. Andersson, Wouter van der Wijngaarta, P. Nilssonb, P. Enoksson, G. Stemme, *Sens. Actuators B* **72**, 259–265 (2001)
- M. Bu, T. Melvin, G. Ensell, J.S. Wilkinson, A.G.R. Evans, J. *Micromechanics Microengineering* **13**(4), S125–S130 (2003)
- L. Cao, S. Mantell, D. Polla, *Sens. Actuators A* **94**, 117–125 (2001)
- J.J. Carr, J.M. Brown, *Introduction to Biomedical Equipment Technology*, 4th edn. (Prentice Hall, Upper Saddle River, NJ, 2001)
- O. Francais, I. Dufour, *Sens. Actuators A* **70**, 56–60 (1998)
- B. Husband, M. Bu, A.G.R. Evans, T. Melvin, J. *Micromechanics Microengineering* **14**, S64–S69 (2004)
- G.S. Jan, *Sens. Actuators A* **21–23**, 203–206 (1990)
- D.J. Laser, J.G. Santiago, J. *Micromechanics Microengineering* **14**(6), R35–R64 (2004)
- D.-S. Lee, J.S. Ko, Y.T. Kim, Bidirectional pumping properties of a peristaltic piezoelectric micropump with simple design and chemical resistance. *Thin Solid Films* **486**, 285–290 (2004)
- C.-S. Liao, G.-B. Lee, J.-J. Wu, C.-C. Chang, T.-M. Hsieh, F.-C. Huang, C.-H. Luo, *Biosens. Bioelectron.* **20**, 1341–1348 (2005)
- A.J. Masys, W. Ren, G. Yang, B.K. Mukherjee, *J. Appl. Phys.* **94**(2), 1155–1162 (2003)
- Z. Miqin, T. Desai, M. Ferrari, *Biomaterials* **19**, 953–960 (1998)
- N.-T. Nguyen, X. Huang, T.K. Chuan, *Trans. Am. Soc. Mech. Eng.* **124**, 384–391 (2002)
- S.Y. Oha, H.S. Choia, H.S. Jiea, J.K. Parkb, *Mater. Sci. Eng. C* **24**, 91–94 (2004)
- F. Rodes, in *EDN Design Ideas* (2004) pp. 83–86
- D. Satakea, H. Ebia, N. Okub, K. Matsudaa, H. Takaoc, M. Ashikic, M. Ishidac, *Sens. Actuators B* **83**, 77–81 (2002)
- Y.-C. Shu, *Mater. Trans.* **43**(5), 1037–1044 (2002)
- J.G. Smits, *Sens. Actuators A* **21–23**, 203–206 (1990)
- H. Takaoa, K. Miyamurab, H. Ebib, M. Ashikia, K. Sawadaa, M. Ishidaa, *Sens. Actuators A* **119**, 468–475 (2005)
- R. Tanabe, S. Hata, A. Shimokohbe, *Microelectron. Eng.* **83**, 1646–1650 (2006)
- S.P. Timoshenko, W. Weaver, *Vibration Problems in Engineering*, 4th edn. (Wiley: New York, 1974)
- J.-H. Tsai, L. Lin, *Sens. Actuator A* **97–98**, 665–671 (2002)
- J. Xie, J. Shih, Q. Lin, B. Yang, Y.C. Tai, *Lab Chip* **4**, 495–501 (2004)